Implementation of Microwave Non-Destructive Testing Principle Using UWB Antenna for Breast Tumor Detection

Haryo Dwi Prananto[1,*], Aditia Nur Bakti[1], Wuwus Ardiatna[2], Mohamad Khoirul Anam[1], Elvina Trivida[1], Yoppy[1], Tyas Ari Wahyu Wijanarko[1], Muhammad Imam Sudrajat[1], Hutomo Wahyu Nugroho[3], Dwi Mandaris[3,4], R. Harry Arjadi[1]

[1]Research Center for Electrical Technology, National Research and Innovation Agency (BRIN), 15314 Tangerang Selatan, Indonesia
[2]Research Center for Equipment Manufacturing Technology, National Research and Innovation Agency (BRIN), 15314 Tangerang Selatan, Indonesia
[3]Directorate of Laboratory Management, Research, Facilities, and Science and Technology, National Research and Innovation Agency (BRIN), 10340 Jakarta, Indonesia
[4]Departement of Electrical Engineering, Mercu Buana University, Jakarta, Indonesia

*Author to whom correspondence should be addressed:
E-mail: hary011@brin.go.id

(Received June 06, 2025; Revised August 01, 2025; Accepted December 17, 2025)

Abstract: Microwave Non-Destructive Testing operates based on the principle of detecting variations in dielectric constants to characterize the internal structure of dielectric materials. Microwave scattering's ability to penetrate biological tissues and differentiate dielectric contrasts enables the detection of tumors within the human breast. In this research, breast tumor detection was performed using an Ultra-Wideband (UWB) antenna, specifically a Metamaterial-Corrugated Antipodal Vivaldi Antenna (MCAVA), operating within the 2–8 GHz frequency range. Materials with dielectric constant values equivalent to those of breast tissue and tumors were employed. Time-domain analysis of S-parameter data obtained from MCAVA antenna measurements reveals the presence of tumor within breast tissue.

Keywords: breast tumor detection; dielectric constant; Metamaterial-Corrugated Antipodal Vivaldi Antenna; Microwave Non-Destructive Testing; UWB antenna

1. Introduction

Cancer is the second leading cause of death worldwide. Data from the International Agency for Research on Cancer shows that approximately 19.3 million new cancer cases occurred in 2020. Among other cancers, female breast cancer has the highest rate, which contributes 11.7% (2.3 million) of the total new cancer cases. Furthermore, the high fatality rate of breast cancer has also led to 685,000 deaths in 2020 [1–3]. In Indonesia, breast cancer also dominated the statistics. In 2022, there a 66,271 (16.2%) new breast cancer cases diagnosed in Indonesia [4]. The late detection of breast tumors (before they develop into cancer) is the major contributor to the high number of deadly cancer cases [5]. Therefore, implementing early breast tumor detection is very crucial for the effective treatment process, particularly to avoid the tumor progressing to more critical stages.

To support this, non-invasive detection techniques have emerged as valuable methods in identifying abnormalities within breast tissue at an early stage without causing discomfort or harm to the patients. One such emerging technique is microwave-based diagnostics. This method has several advantages, including being non-ionizing and non-invasive [6], meaning it does not cause harm to the body and is safe for pregnant women [7–9]. Additionally, it can be performed repeatedly and has relatively low production and operational costs [10].

The use of the microwave for tumor detection is based on the principle of microwave scattering in the breast and utilizes differences in dielectric constants within body tissues to distinguish between healthy tissue and the presence of a tumor [6,11]. This is similar to the microwave nondestructive testing method, which relies on dielectric constant differences to detect defects in non-metallic materials [12–14] or detects a buried object [15–17].

Additionally, several studies on breast cancer detection

Cite: H. Prananto et al., "Implementation of Microwave Non-Destructive Testing Principle Using UWB Antenna for Breast Tumor Detection". Evergreen, 12 (04) 2207-2215 (2025). https://doi.org/10.5109/7402649.

also apply time-domain analysis [18–21]. This method allows for the identification of tumors based on the amplitude of the reflected waves. Focuses on how the signal changes over time. This technique is very useful for detecting transient events like tumor reflection and detecting the tumor location. Motivated by the effectiveness of this approach, the method developed in this research also uses time-domain graph analysis and microwave non-invasive diagnosis as a basis to identify and locate breast tumors.

One of the limitations of the methods in the previous studies is the use of the near-field probes as tumor detection sensors, which may cause contact discomfort or skin irritations. In correlation to these limitations, some studies have explored the use of ultra-wideband (UWB) antennas as the sensing element for tumor detection, including circular patch [22], rectangular patch [23], log periodic [24], metamaterial [25], and Vivaldi [26–29].

Vivaldi antenna has high potential for breast cancer detection applications due to its UWB characteristics [29] and directional [28]. Concerning these advantages, the antenna developed in this study is designed based on an antipodal Vivaldi antenna. In tumor detection using microwave, gain is one of the key components that affects antenna performance. Antennas with higher gain focus energy more effectively, producing stronger signals that improve image clarity, enhance detail detection, less interference, and extend detection range [30][31]. Table 1 presents information from previous studies involving four antennas with different gain values. In addition to the gain variation, changes were also observed in the size of the detected tumors. In these cases, higher gain antennas demonstrated improved detection capabilities, as indicated by the ability to detect smaller tumor sizes.

However, based on the important of gain, to increase the gain, this study made some modifications to the antenna design. This enhanced gain aims to better penetrate the breast phantom skin made from polylactic acid (PLA). The antipodal Vivaldi antenna is designed to operate within the 2 – 8 GHz frequency range. Meanwhile, the skin breast phantom used is constructed from PLA material, shaped using 3D printing technology as its container, where the breast tissue phantom and tumor are made from equivalent materials.

Table 1: Comparison from 4 antennas with different gain and ability of detectable tumor size detection

Antenna Type	Frequency Range (Bandwidth) (GHz)	Peak Gain (dBi)	Detectable Tumor Size Detection (mm)
UWB Antipodal Vivaldi [32]	3.6 – 13	9.27	0.9
UWB Antipodal Vivaldi [33]	3.05 – 12.2	8.3	2
UWB Vivaldi [34]	3 - 10	6	2.5
Tapered Slot UWB Vivaldi [35]	2.79 – 16.66	5	10

2. Method and experimental setup

2.1. Design of Antipodal Vivaldi Antenna

In this study, the Antipodal Vivaldi UWB antenna is modified to achieve higher gain compared to a conventional antipodal Vivaldi. Several techniques can be employed to enhance the gain of an antipodal Vivaldi such as antenna slots [36], corrugated, and metamaterial [37,38], array [39,40], substrate, dielectric lens, and substrate-integrated waveguide [41].

This study proposed metamaterials and corrugations techniques to increase the antenna gain. The design parameters for the antipodal Vivaldi antenna are shown in Table 1. The design of an Antipodal Vivaldi antenna is influenced by its inner and outer edge tapers, which are calculated as follows.

$$y = C_1 e^{\tau} + C_2 \quad (1)$$

In this context, y refers to the curve and τ indicates its tapered rate constant. With the antenna's geometrical parameters, C_1 and C_2 can be derived using the following calculations

$$C_1 = \frac{y_1 - y_1}{e^{\tau x_1} - e^{\tau x_2}} \quad (2)$$

$$C_2 = \frac{y_1 e^{\tau x_2} - y_2 e^{\tau x_1}}{e^{\tau x_2} - e^{\tau x_1}} \quad (3)$$

Meanwhile, (x_1, y_1) represent the starting coordinates and (x_2, y_2) represent the ending coordinates of the curves. Then the length and the other parameter from Antipodal Vivaldi Antenna are shown in Table 1.

Schematic design of the proposed antenna is illustrated in Figure 1. The corrugated are applied in the 2 side of antenna and metamaterials are attached at the Vivaldi antenna to support gain enhancement as shown in Fig 1. The proposed antenna (Metamaterial-Corrugated Antipodal Vivaldi Antenna) is then fabricated over FR4 substrate material due to its low permittivity[42].

A comparison of the S_{11} characteristics between the proposed design and the conventional antipodal Vivaldi antenna is shown in Figure 2. The S_{11} simulation is done using CST microwave studio. From the simulation results, both conventional and proposed design showed can fulfils the bandwidth requirement in this research, in range of 2 – 8 GHz. The proposed design with corrugated elements and metamaterials successfully maintain the bandwidth. The existence of metamaterials did not affect the bandwidth

Table 2: Parameters of the proposed design antipodal Vivaldi antenna

Parameters	Dimensions (mm)
L	95
W	100
Tapered rate constant (τ)	0.1
La	62
Wn	3
D	1.875
Da	0.75

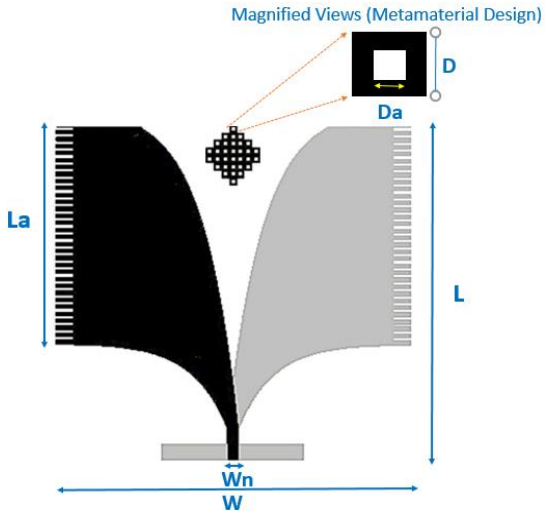

Fig. 1: Proposed Design of Antipodal Vivaldi

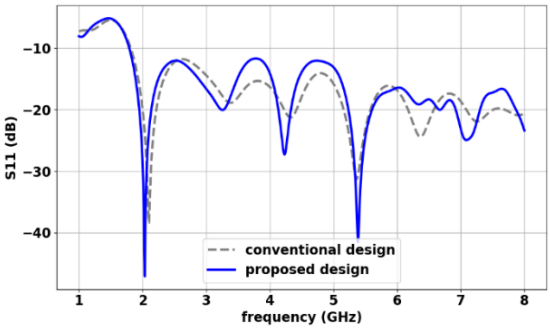

Fig. 2: S_{11} characteristics of proposed and conventional design antipodal Vivaldi antenna

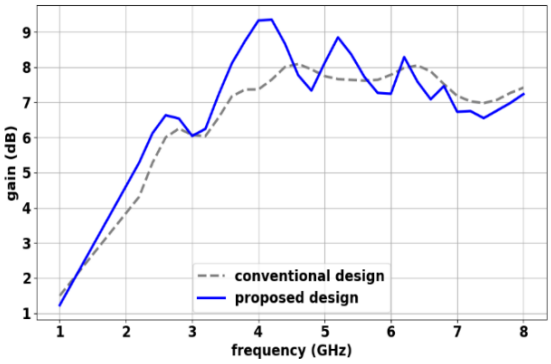

Fig. 3: Gain Comparison from Simulation between Conventional and Proposed Design

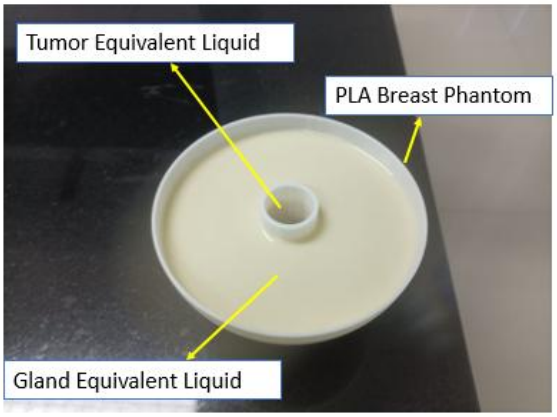

Fig. 4: Breast and Tumor Phantom

range due to their electrically smaller size compared to resonant wavelength of Vivaldi antenna. Metamaterials with their inductive nature compensates the capacitance from the antenna. This leads to a maximum power transfer to the Antipodal Vivaldi antenna, thus increasing the antenna gain for most of the antenna's bandwidth (especially in the 2 - 6 GHz range), as shown in Figure 3.

2.2. Breast and tumor phantom

The breast phantom and tumor in this study use materials according from this research [43], with dielectric constant values equivalent to actual body tissues. This study considers only two breast tissue components: the gland, representing the breast, and the tumor. The container for the breast and tumor phantom was printed using 3D printing with PLA filament with diameter 11 cm The gland material was prepared using a mixture of 50 ml deionized water, 6 g NaCl, and 30 g wheat flour, while the tumor material consisted of 100 ml deionized water and 8 g NaCl. The result of mixing process for both the gland and tumor phantoms is shown in Figure 4.

2.3. Verification constant dielectric from the phantom

The breast tumor detection system using microwaves is based on detecting microwave scattering variations in different materials, influenced by differences in dielectric constants. Therefore, to ensure a difference in dielectric constants in the fabricated phantoms, verification of dielectric characteristics was conducted. Based on previous research, dielectric constant characteristics can be measured using metamaterial split-ring resonators[44,45]. Therefore, in this study, the dielectric constant characteristics are measured using a split-ring resonator. Measurements were performed using a complementary split-ring resonator, as shown in Figure 5. The gland and tumor phantoms were placed in a container, which was then positioned on top of the sensor. The sensor operates at a cutoff frequency of 1.9 GHz. Verification was carried out by analyzing the difference in dielectric constants through variations in the cutoff frequency of the two

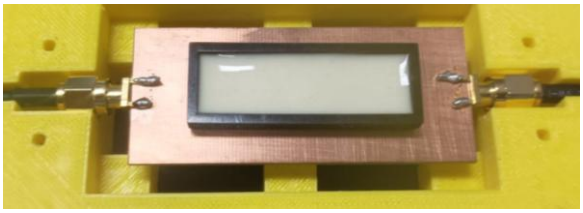

Fig. 5: Measurement of the characteristic of a constant dielectric from a phantom

phantoms.

2.4. Breast tumor detection setup

Figure 6 shows the measurement setup for the tumor detection system by implementation microwave non-destructive testing method [13,14]. The Microwave Non Destructive Testing method used is microwave reflectometry. The working principle of this method can be seen in Figure 6 [13)15)] The antenna/probe is placed at a far-field distance from the material under test, where the far-field distance depends on the antenna dimensions and the minimum operating frequency. In this case, the propagation medium between the antenna and the material under test is air. The material under test is also positioned at a distance from a reference metal plate, with air serving as the separating medium. The measurement parameter used in this method is S_{11}, which reflects the propagation path of the signal: from the antenna, through air, the material under test, and air again, before being reflected by the metal plate. In addition to serving as the object that reflects the antenna's propagation in the S_{11} measurement, the metal plate also functions as a reference and a marker to indicate the position and representation of the material under test. This is because the propagation from the antenna is fully reflected upon striking the metal plate. Apart from that, the metal plate also has a function in limiting the possibility of noise/interference from electromagnetic waves originating from the surrounding environment.

The reflected signal is then captured by the same antenna/probe. The S_{11} propagation from the antenna passes through different media and materials, where variations in dielectric constants can cause changes in the measured S_{11} values. As a result, defects in the material under test can be identified based on these changes.

Following the principle of the non-destructive testing method as illustrated in Figure 6, the principle is then implemented for tumor detection, as shown in Figure 7. Before measurements are taken, the ports on the network analyzer are calibrated first. Then, the antenna connected to a port in a Vector Network Analyzer. The antenna is placed facing each other with the breast and tumor phantom, the opposite side the metal facing the breast and phantom tumor. The length of metal is 20 cm. The measurement is conducted using scattering parameter S_{11}, where one antenna functions as the transmitter and the

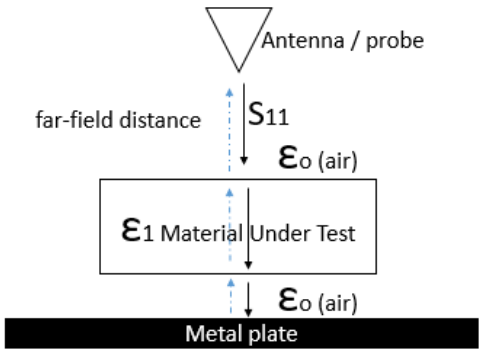

Fig. 6: Principle of Microwave Non-Destructive Testing Method

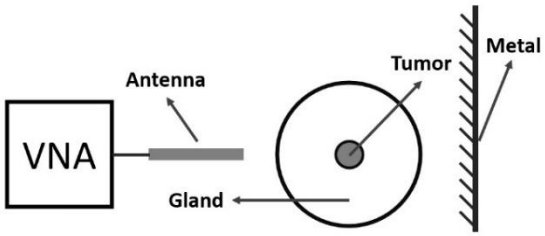

Fig. 7: Measurement setup

receiver. The distance between the antenna and the breast phantom is 1 cm. Therefore, the distance from metal to breast and tumor phantom is 10 cm. For data collection, the breast and tumor phantom was moved vertically from one metal end to the other as shown in Figure 6, taking data every 1 cm of phantom displacement. The difference in S_{11} values caused by the variation in dielectric constants between the tumor and breast tissue (glandular) will indicate the presence or absence of a tumor in the breast.

In this study, time-domain measurement data is also collected to detect the presence and position of the tumor. In the S_{11} converter settings on the network analyzer, the windowing used is the Kaiser window with minimum parameters, which is useful for filtering the noise produced during measurements. Time-domain measurements are obtained from the vector network analyzer, where theoretically, the time-domain response is derived from the IFFT transformation of the antenna's S_{11} data. The time domain is utilized because, in this domain, the position of the tumor can be identified. The result of this domain is a plot of time versus measured amplitude, where the time can be used to calculate distance, and changes in the amplitude indicate variations in the dielectric constant of the material under test—in this case, a tumor within the breast (glandular tissue).

3. Results and discussion

This chapter discusses the results of the characteristics of metamaterial-corrugated antipodal Vivaldi antenna, the verification of dielectric constant characteristics, the S_{11}

measurement of the breast phantom with and without a tumor, and the inverse time-domain graph and mapping derived from the measured S_{11} graph.

3.1. Characteristics of Metamaterial-Corrugated Antipodal Vivaldi Antenna

The result of fabrication of Metamaterial-Corrugated Antipodal Vivaldi Antenna (MCAVA) is shown in Figure 8. In Figure 9, a comparison of the S_{11} measurement results and simulation for the MCAVA is presented. It was observed that the measurement results are generally optimal, though performance is slightly suboptimal in the 4.6 – 4.8 GHz range. Figure 10 shows the comparison of gain between simulation and measurement. It can be seen that there is a similarity in the trend of both graphs, although the values differ at each frequency. This discrepancy of can likely be attributed to variations in the dielectric constant of the substrate and copper, as well as imperfections in the fabrication process. As shown in previous studies [46], variations in the dielectric constant of the fabricated antenna can significantly affect both S_{11} and gain. Fabrication imperfections, such as errors during the etching process or PCB printing, can cause surface irregularities or dimensional changes in the copper layer. In addition, imperfections can also be influenced by the manual soldering process of the antenna with the connector. These defects can the impedance matching of antenna and it can change or shift in the S_{11} and gain performance [47].

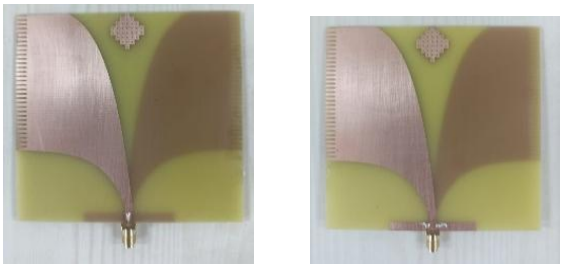

(a) (b)

Fig. 8: Fabrication of MCAVA in (a) top view and (b) bottom view

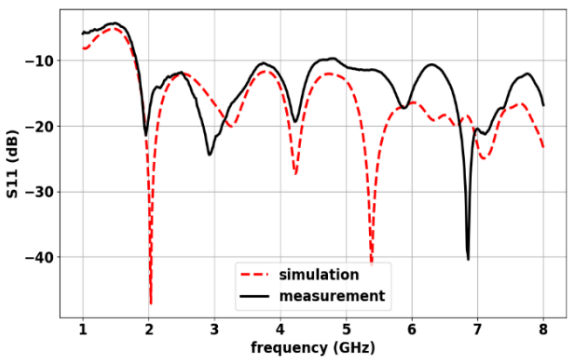

Fig. 9: S_{11} from Metamaterial-Corrugated Antipodal Vivaldi Antenna

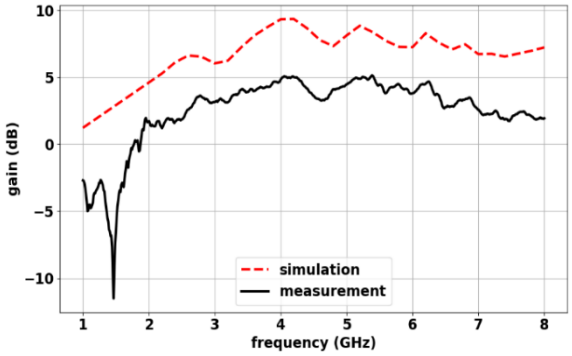

Fig. 10: Gain measurement of the MCAVA

3.2. Verification characteristics of the dielectric constant of breast and tumor tissue

The graph shown in Figure 11 represents the measurement results of the dielectric constant characteristics of the fabricated phantom. The results of the negative peak values between the gland tissue phantom and the tumor tissue, around 1.8 GHz, where the gland peak at 1.825 GHz with peak of S_{21} value is -38.776 and the tumor at 1.843 GHz with S_{21} value of -36.436, that indicate a difference. This verifies that the two fabricated tissue phantoms have different dielectric constant values and can be used as phantoms in this study.

3.3. Breast tumor detection

Figure 12 shows the experimental setup of the breast tumor detection. It is the representation from measurement setup in Figure 7. The S_{11} mapping results along the breast and tumor phantom positions, obtained by shifting the phantom 1 cm along the metal plate dimension, were then transformed into the time domain using the Inverse Fast Fourier Transform (IFFT) method. A mapping of this data is then presented in Figure 13.

The minimum detectable tumor size can be obtained by using the time domain resolution and depends on the frequency range and windowing of the time domain measurement. In this paper, the calculated time domain resolution (td) is 75 ps. If this value is used in the calculation for distance resolution, td x c x 0.66, where c is the speed of light and 0.66 is the velocity factor of the coaxial cable, the distance resolution can be obtained as 15 mm. For the S_{11} measurement, the distance resolution is halved; therefore, the distance resolution of the measurement is around 7.5 mm. This distance resolution is related to the minimum size of the tumor detection.

Figure 13 shows the mapping results for three conditions: when the phantom measured was solely the PLA breast phantom container, the gland without a tumor, and the gland with a tumor. In each image, around time domain index 5, a large dB value is visible, indicating the antenna's proximity to the outer part of the phantom. Meanwhile, at a time domain index around 43, a large amplitude value of approximately 45 dB suggests the presence of metal. This

is due to the high reflected power from the S_{11} measurement, which only occurs when electromagnetic waves strike a metal plate.

Comparing the three Figures reveals differences in the central region, specifically around coordinates (x, y; 7, 25). This indicates the detection of a tumor positioned in the central part of the phantom. The presence of the tumor is shown by varying amplitude values in the central section across each Figure. The amplitude difference observed in Figure 13 (b) and (c) signifies a difference in dielectric

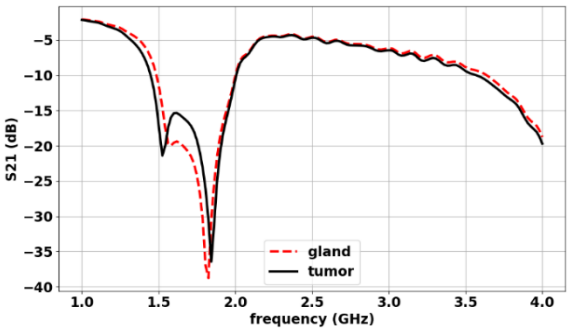

Fig. 11: Graph of dielectric constant characteristic from 2 phantoms

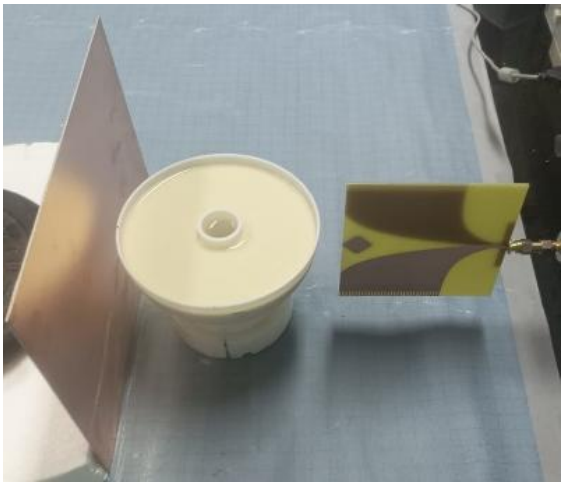

Fig. 12: Measurement of Breast Tumor Detection

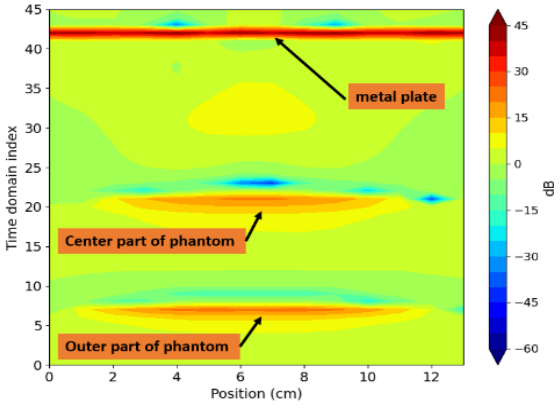

(a)

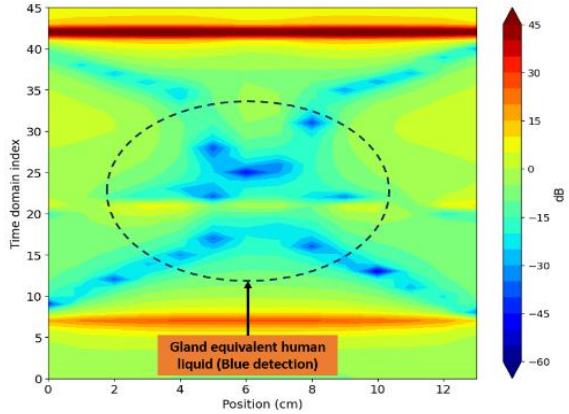

(b)

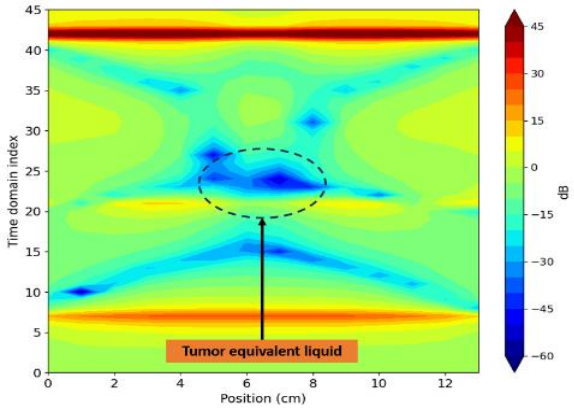

(c)

Fig. 13: Mapping of time domain analysis from (a) PLA Breast phantom (without gland and tumor phantom) (b) Gland without Tumor Phantom (c) Gland with Tumor Phantom

constant values between the gland (breast) and the tumor. This amplitude variation demonstrates that a tumor can be detected using the microwave non-destructive testing method implemented in this study.

4. Conclusion

An experiment on breast tumor detection has been conducted using time-domain graph analysis in accordance with the principles of microwave non-destructive testing. An UWB antenna type of Antipodal Vivaldi modified with corrugated and combined with metamaterials is used to increase of gain characteristics. The presence and position of the tumor is observed from the time-domain analysis mapping calculated from of the S_{11} measurement. Based on the experiment, tumor detection can be performed using microwave non-destructive testing.

Acknowledgements

This work was supported by the Research and Innovation for Advanced Indonesia (RIIM) Batch 4 Grant, funded by the Indonesian Government under B-3837/II.7.5/FR.06.00//11/2023 agreement.

References

1) D. Khanikar, K. Kamalasanan, A. Krishnamurthy, M. Hazarika, and A.C. Kataki, "Breast Cancer," in: A.C. Kataki, D. Barmon (Eds.), Fundamentals in Gynaecologic Malignancy, Springer Nature Singapore, Singapore, 2022: pp. 133–181. doi:10.1007/978-981-19-5860-1_10.
2) H. Sung, J. Ferlay, R.L. Siegel, M. Laversanne, I. Soerjomataram, A. Jemal, and F. Bray, "Global cancer statistics 2020: globocan estimates of incidence and mortality worldwide for 36 cancers in 185 countries," CA A Cancer J Clinicians, 71 (3) 209–249 (2021). doi:10.3322/caac.21660.
3) S.R. Anggita, and F.R. Pratama, "Texture-based classification of benign and malignant mammography images using weka machine learning : an optimal approach texture-based classification of benign and malignant mammography images using weka machine learning : an optimal approach," Evergreen, 10 (3) 1570–1580 (2023). doi:https://doi.org/10.5109/7151705.
4) J. Ferlay, M. Ervik, F. Lam, M. Laversanne, M. Colombet, L. Mery, M. Piñeros, A. Znaor, I. Soerjomataram, and F. Bray, "Global Cancer Observatory: Cancer Today," International Agency for Research on Cancer, Lyon, France, 2025. https://gco.iarc.who.int/today.
5) H. Sumarti, Sheilla Rully Anggita, Hartono, Fachrizal Rian Pratama, and Alvania Nabila Tasyakuranti, "Texture-based classification of benign and malignant mammography images using weka machine learning: an optimal approach," Evergreen, 10 (3) 1570–1580 (2023). doi:10.5109/7151705.
6) M.A. Aldhaeebi, K. Alzoubi, T.S. Almoneef, S.M. Bamatraf, H. Attia, and O.M. Ramahi, "Review of microwaves techniques for breast cancer detection," Sensors, 20 (8) 2390 (2020). doi:10.3390/s20082390.
7) D. Álvarez Sánchez-Bayuela, J. Fernández Martín, G. Tiberi, N. Ghavami, R. Giovanetti González, L.M. Cruz Hernánez, P.M. Aguilar Angulo, A.D. Martínez Gómez, A. Rodríguez Sánchez, A. Bigotti, B. Khalesi, L. Pontoriero, M. Calabrese, A.S. Tagliafico, and C. Romero Castellano, "Microwave imaging for breast cancer screening: protocol for an open, multicentric, interventional, prospective, non-randomised clinical investigation to evaluate cancer detection capabilities of mammowave system on an asymptomatic population across multiple european countries," BMJ Open, 14 (11) e088431 (2024). doi:10.1136/bmjopen-2024-088431.
8) L. Wang, "Microwave imaging and sensing techniques for breast cancer detection," Micromachines, 14 (7) 1462 (2023). doi:10.3390/mi14071462.
9) J. Qi, and Z. Li, "Non-destructive testing of human teeth using microwaves: a state-of-the-art review," Journal of Electrical Engineering, 74 (1) 40–47 (2023). doi:10.2478/jee-2023-0005.
10) M. Lu, X. Xiao, Y. Pang, G. Liu, and H. Lu, "Detection and localization of breast cancer using uwb microwave technology and cnn-lstm framework," IEEE Trans. Microwave Theory Techn., 70 (11) 5085–5094 (2022). doi:10.1109/TMTT.2022.3209679.
11) W. Saleh, and N. Qaddoumi, "Potential of near-field microwave imaging in breast cancer detection utilizing tapered rectangular waveguide probes," Computers & Electrical Engineering, 35 (4) 587–593 (2009). doi:10.1016/j.compeleceng.2008.08.005.
12) H.T. Andhyka, "Effects of polarization and different tissue on terahertz cancer imaging effects of polarization and different tissue on terahertz cancer imaging," Evergreen, 11 (1) 525–535 (2024). doi:https://doi.org/10.5109/7172318.
13) A. Ghattas, R. Al-Sharawi, A. Zakaria, and N. Qaddoumi, "Detecting defects in materials using nondestructive microwave testing techniques: a comprehensive review," Applied Sciences, 15 (6) 3274 (2025). doi:10.3390/app15063274.
14) M. Saif Ur Rahman, M.A. Abou-Khousa, and M. Firdaus Akbar, "A review on microwave non-destructive testing (ndt) of composites," Engineering Science and Technology, an International Journal, 58 101848 (2024). doi:10.1016/j.jestch.2024.101848.
15) Y. Fang, X. Yang, H. Chen, Z. Chen, R. Wang, Y. Li, and S. Xie, "Non-destructive quantitative evaluation of delamination depth and thickness in gfrp using microwave reflectometry," NDT & E International, 144 103065 (2024). doi:10.1016/j.ndteint.2024.103065.
16) G.N. Jawad, and M.F. Akbar, "IFFT-based microwave non-destructive testing for delamination detection and thickness estimation," IEEE Access, 9 98561–98572 (2021). doi:10.1109/ACCESS.2021.3095105.
17) J. Takayama, Y. Ohara, and W. Sun, "Nondestructive evaluation of air voids in concrete structures using microwave radar technique," SICE Journal of Control, Measurement, and System Integration, 15 (1) 36–47 (2022). doi:10.1080/18824889.2021.2019968.
18) C. Blanco-Angulo, A. Martínez-Lozano, R. Gutiérrez-Mazón, C.G. Juan, H. García-Martínez, J. Arias-Rodríguez, J.M. Sabater-Navarro, and E. Ávila-Navarro, "Non-invasive microwave-based imaging system for early detection of breast tumours," Biosensors, 12 (9) 752 (2022).

doi:10.3390/bios12090752.

19) Y. Rahayu, M. Kahiron, K.N.A.R. Rani, and T. Praludi, “Detection of breast tumour depth using felt substrate textile antenna,” ARASET, 39 (1) 59–75 (2024).
20) Y. Rahayu, R. Rosdiansyah, M.F. Hilmi, and T. Odih, “Wearable antenna for time-domain breast tumor detection,” IJTech, 12 (6) 1101 (2021). doi:10.14716/ijtech.v12i6.5187.
21) D.N. Elsheakh, R.A. Mohamed, O.M. Fahmy, K. Ezzat, and A.R. Eldamak, “Complete breast cancer detection and monitoring system by using microwave textile based antenna sensors,” Biosensors, 13 (1) 87 (2023). doi:10.3390/bios13010087.
22) A.E. Fatimi, S. Bri, and A. Saadi, “UWB antenna with circular patch for early breast cancer detection,” TELKOMNIKA, 17 (5) 2370 (2019). doi:10.12928/telkomnika.v17i5.12757.
23) N. Hammouch, A. Rghioui, H. Ammor, M. Oubrek, and J. Lloret, “A low-cost uwb microwave imaging system for early-stage breast cancer detection,” Multimed Tools Appl, 84 (17) 17329–17360 (2024). doi:10.1007/s11042-024-19761-0.
24) A. Syed, N. Sobahi, M. Sheikh, R. Mittra, and H. Rmili, “Modified 16-quasi log periodic antenna array for microwave imaging of breast cancer detection,” Applied Sciences, 12 (1) 147 (2021). doi:10.3390/app12010147.
25) M.A. Aldhaeebi, T. Almoneef, S. Bamatraf, A.O. Aldhaibain, O. Bakhalah, S. Alhdad, S. Bakhalah, and M.K. Saleem, “Near-field metasurface sensor for an early-stage breast cancer detection,” Sensors International, 6 100305 (2025). doi:10.1016/j.sintl.2024.100305.
26) S. Tangwachirapan, W. Thaiwirot, and P. Akkaraekthalin, “Design and analysis of antipodal vivaldi antennas for breast cancer 燚 etection,” Computers, Materials & Continua, 73 (1) 411–431 (2022). doi:10.32604/cmc.2022.028294.
27) H. Özmen, and M.B. Kurt, “Radar-based microwave breast cancer detection system with a high-performance ultrawide band antipodal vivaldi antenna,” Turk J Elec Eng & Comp Sci, 29 (5) 2326–2345 (2021). doi:10.3906/elk-2010-49.
28) M. Slimi, B. Jmai, H. Dinis, A. Gharsallah, and P.M. Mendes, “Metamaterial vivaldi antenna array for breast cancer detection,” Sensors, 22 (10) 3945 (2022). doi:10.3390/s22103945.
29) M.-A. Boujemaa, R. Herzi, F. Choubani, and A. Gharsallah, “UWB antipodal vivaldi antenna with higher radiation performances using metamaterials,” Appl. Phys. A, 124 (10) 714 (2018). doi:10.1007/s00339-018-2132-1.
30) A. Gupta, S. Kumar Yadav, A.D. Durai C, V. Kuamr, M.H. Alsharif, P. Uthansakul, and M. Uthansakul, “Enhanced breast tumor localization with dra antenna backscattering and gpr algorithm in microwave imaging,” Results in Engineering, 24 103044 (2024). doi:10.1016/j.rineng.2024.103044.
31) T. Saeidi, S.N. Mahmood, S. Saleh, N. Timmons, A.J.A. Al-Gburi, and F. Razzaz, “Ultra-wideband (uwb) antennas for breast cancer detection with microwave imaging: a review,” Results in Engineering, 25 104167 (2025). doi:10.1016/j.rineng.2025.104167.
32) Ş. Yıldız, and M.B. Kurt, “Breast cancer detection using a high-performance ultra-wideband vivaldi antenna in a radar-based microwave breast cancer imaging technique,” Applied Sciences, 15 (11) 6015 (2025). doi:10.3390/app15116015.
33) H. Özmen, and M.B. Kurt, “Radar-based microwave breast cancer detection system with a high-performance ultrawide band antipodal vivaldi antenna,” Turk J Elec Eng & Comp Sci, 29 (5) 2326–2345 (2021). doi:10.3906/elk-2010-49.
34) A.M. Qashlan, R.W. Aldhaheri, and K.H. Alharbi, “A modified compact flexible vivaldi antenna array design for microwave breast cancer detection,” Applied Sciences, 12 (10) 4908 (2022). doi:10.3390/app12104908.
35) S. Sasikala, K. Karthika, S. Arunkumar, K. Anusha, S. Adithya, and A.J.A. Al-Gburi, “Design and analysis of a low-profile tapered slot uwb vivaldi antenna for breast cancer diagnosis,” PIER M, 124 43–51 (2024). doi:10.2528/PIERM23110702.
36) M. Pradesh, and C. Engineering, “Design and development of machine learning assisted cylindrical dielectric resonator antenna,” Evergreen, 10 (01) 308–316 (2023).
37) S. El-Nady, H.M. Zamel, M. Hendy, A.H.A. Zekry, and A.M. Attiya, “GAIN enhancement of a millimeter wave antipodal vivaldi antenna by epsilon-near-zero metamaterial,” PIER C, 85 105–116 (2018). doi:10.2528/PIERC18050302.
38) A.S. Dixit, and S. Kumar, “Gain enhancement of antipodal vivaldi antenna for 5g applications using metamaterial,” Wireless Pers Commun, 121 (4) 2667–2679 (2021). doi:10.1007/s11277-021-08842-0.
39) H. Liu, W. Yang, A. Zhang, S. Zhu, Z. Wang, and T. Huang, “A miniaturized gain-enhanced antipodal vivaldi antenna and its array for 5g communication applications,” IEEE Access, 6 76282–76288 (2018). doi:10.1109/ACCESS.2018.2882914.
40) S. Kumar, and K.V.S.R. Murthy, “A quad element textile material based printed mimo antenna for wearable application,” Evergreen, 11 (02) 1268–1272 (2024).
41) A.S. Dixit, and S. Kumar, “A survey of performance

enhancement techniques of antipodal vivaldi antenna," IEEE Access, 8 45774–45796 (2020). doi:10.1109/ACCESS.2020.2977167.

42) Achyut Sharma, Sanyog Rawat, and Sunil Kumar Khah, "Annular rings antenna for wimax / wlan band with frequency and polarization diversity," Evergreen, 11 (4) 3156–3163 (2024). doi:10.5109/7326953.
43) F.-E. Zerrad, M. Taouzari, E.M. Makroum, S. Ahmad, F.O. Alkurt, M. Karaaslan, M.T. Islam, and M.I. Hussein, "Symmetrical and asymmetrical breast phantoms with 3d-printed anatomical structure for microwave imaging of breast cancer," IEEE Access, 10 96896–96908 (2022). doi:10.1109/ACCESS.2022.3205004.
44) A. Buragohain, G.S. Das, Y. Beria, A.J.A. Al-Gburi, P.P. Kalita, and T. Doloi, "Highly sensitive differential hexagonal split ring resonator sensor for material characterization," Sensors and Actuators A: Physical, 363 114704 (2023). doi:10.1016/j.sna.2023.114704.
45) X. Han, K. Liu, S. Zhang, P. Peng, C. Fu, L. Qiao, and Z. Ma, "CSRR metamaterial microwave sensor for measuring dielectric constants of solids and liquids," IEEE Sensors J., 24 (9) 14167–14176 (2024). doi:10.1109/JSEN.2024.3373755.
46) F. Oktafiani, E.Y. Hamid, and A. Munir, "Wideband dual-polarized 3d printed quad-ridged horn antenna," IEEE Access, 10 8036–8048 (2022). doi:10.1109/ACCESS.2022.3143164.
47) K. Berry, E.M. Brown, B. Pothier, S. Fedorka, A. Akyurtlu, C. Armiento, G.F. Walsh, and C. Shemelya, "Overcoming variability in printed rf: a statistical method to designing for unpredictable dimensionality," Designs, 6 (1) 13 (2022). doi:10.3390/designs6010013.